Simulations of thermionic suppression during tungsten transient melting experiments

M. Komm[1], P. Tolias[2], S. Ratynskaia[2], R. Dejarnac[1], J. P. Gunn[3], K. Krieger[4], A. Podolnik[1,5], R. A. Pitts[6] and R. Panek[1]

[1] Institute of Plasma Physics CAS, Za Slovankou 3, 182 00 Prague 8, Czech Republic
[2] KTH Royal Institute of Technology, Space & Plasma Physics, SE-10044 Stockholm, Sweden
[3] CEA, IRFM, F-13108 Saint-Paul-lez-Durance, France
[4] Max-Planck-Institut für Plasmaphysik, 85748 Garching b. München, Germany
[5] MFF Charles University, V Holešovičkách 2, 180 00 Prague 8, Czech Republic
[6] ITER Organization, Route de Vinon-sur-Verdon, CS 90 046, 13067 St. Paul Lez Durance, France

E-mail: komm@ipp.cas.cz

Abstract. Plasma-facing components receive enormous heat fluxes under steady state and especially during transient conditions that can even lead to tungsten (W) melting. Under these conditions, the unimpeded thermionic current density emitted from the W surfaces can exceed the incident plasma current densities by several orders of magnitude triggering a replacement current which drives melt layer motion via the $\boldsymbol{J} \times \boldsymbol{B}$ force. However, in tokamaks, the thermionic current is suppressed by space-charge effects and prompt re-deposition due to gyro-rotation. We present comprehensive results of particle-in-cell modelling using the 2D3V code SPICE2 for the thermionic emissive sheath of tungsten. Simulations have been performed for various surface temperatures and selected inclinations of the magnetic field corresponding to the leading edge and sloped exposures. The surface temperature dependence of the escaping thermionic current and its limiting value are determined for various plasma parameters; For the leading edge geometry, the results agree remarkably well with the Takamura analytical model. For the sloped geometry, the limiting value is observed to be proportional to the thermal electron current and a simple analytical expression is proposed that accurately reproduces the numerical results.

Keywords: Particle-in-cell, thermionic emission, emissive sheath, space-charge, tungsten, transient melting

1. Introduction

ITER and next step fusion devices risk overheating the metallic plasma-facing components (PFCs) and achieving transient melting even for tungsten, which has the highest melting point of all metals. As a consequence, a concentrated experimental and modelling effort has been put forward in the past years in order to improve the understanding of the effect of molten

PFCs on plasma operation and wall degradation. In dedicated JET [1–3] and AUG [4, 5] experiments, specially designed tungsten lamellae (referred as *special lamellae* further) were exposed in the divertor during high power Type I ELMy H-modes, where transient melting was achieved following repetitive ELM heat load impacts. In both tokamaks, the special lamellae had identical geometry, featuring either a protruding leading edge oriented nearly perpendicular to the magnetic field or a slope at $\alpha = 17.5^\circ$ with respect to the magnetic field.

In the absence of external electromagnetic fields and space-charge generated electrostatic fields, the nominal or unimpeded thermionic current density is described by the Richardson-Dushman formula, $j_{\rm th}^{\rm nom} = A_{\rm eff} T_{\rm s}^2 \exp\left(-W_{\rm f}/kT_{\rm s}\right)$, where $T_{\rm s}$ is the surface temperature, $W_{\rm f} = 4.55\,{\rm eV}$ the work-function and $A_{\rm eff} = 60\,{\rm Acm^{-2}K^{-2}}$ the effective Richardson constant for tungsten [6–8]. At the proximity of the tungsten melting point, not only can $j_{\rm th}^{\rm nom}$ by far exceed the incident plasma currents which leads to emitted electron return under the action of repelling self-consistent fields (virtual cathode) but also the magnetic field inclination can be grazing which leads to emitted electron reabsorption under the action of the Lorentz force (prompt re-deposition). For such scenarios, due to the coexistence and coupling between the two thermionic suppression mechanisms, there are no rigorous theories for the escaping thermionic current or even approximate modifications of the Child-Langmuir law for the limited current [9, 10]. In fact, even the existence of a constant limited current can be debated.

However, dedicated particle-in-cell (PIC) simulations can model the problem with sufficient accuracy. The 2D3V PIC code SPICE2 [11, 12] was recently updated to include the generation of thermionic electrons [13]. In that study, scans were performed in the magnetic field inclination angle for selected surface temperatures and different wall configurations relevant to inter- and intra-ELM conditions of the JET divertor [13] aiming to gain insight into the complex interplay between the two suppression mechanisms. In this contribution, plasma conditions are targeted that correspond to the dedicated AUG experiments and detailed scans in the surface temperatures for inclination angles relevant to the special lamellae are performed. The simulation geometry comprises of an infinite flat surface with magnetic field inclination α, see Fig.1. The main objective is to provide input for the MEMOS code [14, 15], which simulates macroscopic melt layer motion; the escaping thermionic current is central to such simulations, since it drives a strong replacement current through the bulk of the lamella, which is responsible for the dominant $\boldsymbol{J} \times \boldsymbol{B}$ force density acting on the melt.

2. Simulated scenarios

Both inter-ELM and intra-ELM plasma conditions were targeted for the exposure geometries of a protruding lamella with leading edge and a sloped lamella. Deuterium ions and $B = 2.5\,{\rm T}$ were considered. For the inter-ELM plasmas, divertor Langmuir probe measurements in discharge #33511 (where the outer strike point was located at the special lamella) were employed. The electron temperature measured at the radial location of the lamella was $T_{\rm e} = 25\,{\rm eV}$. The electron density was derived from the saturation current to be $n_{\rm e} = 3 \times 10^{19}\,{\rm m^{-3}}$ within the assumptions of $T_{\rm i} = T_{\rm e}$ and $c_{\rm s} = \sqrt{(T_{\rm e} + T_{\rm i})/m_{\rm i}}$. Using $\gamma = 7$ for the sheath heat transmission coefficient, these parameters translate to $q_{\rm top} \simeq 2.0\,{\rm MW/m^2}$ for the top surface

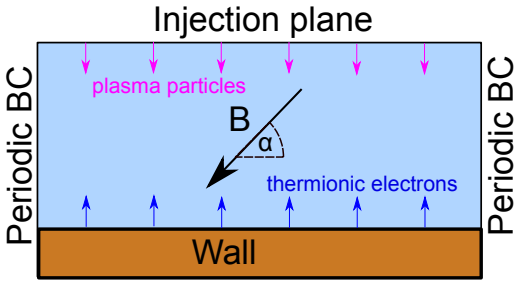

Figure 1. Schematic of the SPICE2 simulation geometry with the particle injection plane located at the top and the hot thermionically emitting wall located at the bottom. The magnetic field is inclined at an angle α with respect to the surface plane.

heat flux, which matches both IR observations and THEODOR calculations. For the intra-ELM plasmas, probe measurements were not available and the local electron temperature was assumed to be $T_\mathrm{e} = 100\,\mathrm{eV}$, which corresponds to $1/5$ of the pedestal temperature [16]. A characteristic peak IR measurement of $q_\mathrm{top} \simeq 20\,\mathrm{MW/m^2}$ was adopted ($q_\parallel \simeq 450\,\mathrm{MW/m^2}$), which led to $n_\mathrm{e} = 4 \times 10^{19}\,\mathrm{m^{-3}}$. Finally, a "reduced" intra-ELM scenario was considered, $T_\mathrm{e} = 60\,\mathrm{eV}$ and $n_\mathrm{e} = 4 \times 10^{19}\,\mathrm{m^{-3}}$ leading to $q_\mathrm{top} \simeq 10\,\mathrm{MW/m^2}$, in an effort to simulate different spatio-temporal regions of the ELM profile.

The surface was assumed to be at a fixed potential $3kT_\mathrm{e}$ below the plasma potential. For each scenario, we performed a series of simulations with varying homogeneous surface temperatures in the range $T_\mathrm{s} = 3400-4500\,\mathrm{K}$ for the leading edge, $T_\mathrm{s} = 3000-4000\,\mathrm{K}$ for the sloped geometry. The selected ranges correspond to realistic lamella temperatures during the exposures and cover the expected transition region, where the thermionic current given by the Richardson-Dushman formula becomes limited due to the formation of the virtual cathode. For the leading edge, the PIC grid size was set equal to $0.0125\lambda_\mathrm{D}$ to properly resolve the potential profile of the virtual cathode (meaning that the potential minimum is at least further than 1 cell above the surface [13]). For the sloped lamella, the PIC grid size could be relaxed to $0.05\lambda_\mathrm{D}$. The W surface is considered to be polycrystalline, atomically clean and perfectly planar.

3. Leading edge geometry

For normal magnetic field incidence, the PIC simulations can be compared with the theoretical description proposed by Takamura *et al.* [17]. This model is valid for arbitrary bias, assumes mono-energetic collisionless ions and takes into account the finite temperature of emitted electrons. It is based on separating the sheath into two regions of monotonic potential profile. The standard Poisson analysis is employed in the region from the sheath entrance to the virtual cathode (where $d\phi/dx = 0$) including the escaping thermionic electron population. The connection with the region from the virtual cathode to the material surface is provided by considering thermionic suppression from the conservative electrostatic field. For $T_\mathrm{s} \neq 0$, the escaping current and the virtual cathode depth can be obtained by solving the system of a cubic equation and a non-linear equation. For $T_\mathrm{s} = 0$, the virtual cathode coincides with

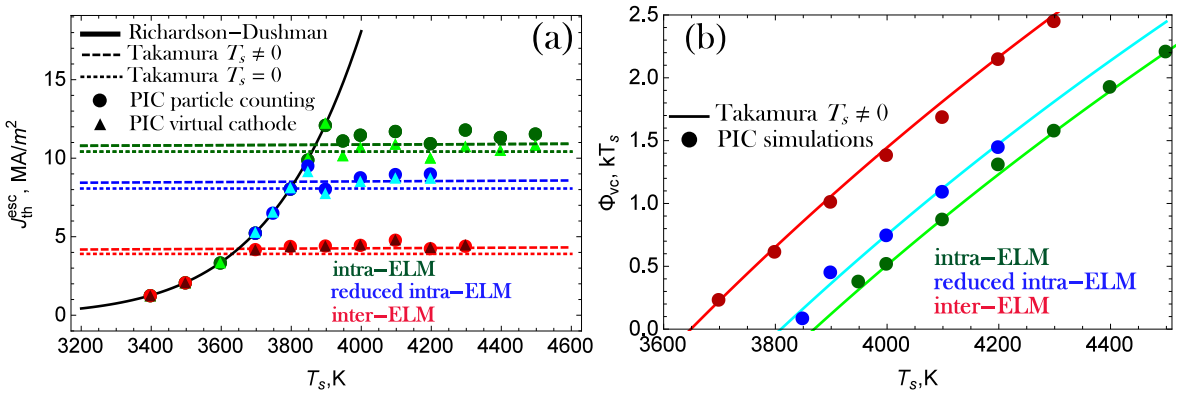

Figure 2. Leading edge geometry results for the selected plasma scenarios. (a) The escaping thermionic current from the PIC simulations as computed by the particle counting method (•) and the virtual cathode method (▲) together with the space-charge limited current as calculated by the Takamura model [17] for $T_s \neq 0$ (dashed lines) and $T_s = 0$ (dotted lines). (b) The virtual cathode depth normalized by the surface temperature resulting from the PIC simulations (•) and the finite-T_s Takamura model (continuous lines).

the material surface and the cubic equation becomes quadratic, which leads to a closed-form expression for the escaping current. We emphasize that the magnitude of the escaping current only slowly approaches the $T_s = 0$ result as the T_e/kT_s ratio increases; even for the large $T_e/kT_s \gtrsim 80$ relevant for the AUG inter and intra-ELM plasmas, the finite-T_s predictions quantitatively differ from the $T_s = 0$ predictions.

In PIC simulations, the escaping thermionic current j_{th}^{esc} can be generally computed by particle counting. For normal magnetic field incidence, owing to the Maxwellian distribution of the thermionic electrons and the conservative nature of the repelling electrostatic potential, the escaping thermionic current is connected to the Richardson-Dushman current through the relation $j_{th}^{esc} = j_{th}^{nom} \exp(-e\Phi_{vc}/kT_s)$, which provides an alternative computation method of j_{th}^{esc} through the virtual cathode depth $\Phi_{vc} = \phi_{vc} - \phi_s$, where ϕ_{vc} is the sheath potential minimum and ϕ_s is the surface potential. Both methods have been followed, as a check of internal consistency. However, small errors in the numerical solution of the Poisson equation correspond to a very small fraction of T_e, which translates to a respectable fraction of T_s and consequently of Φ_{vc} [13]. Therefore, there should be minor differences between the two methods that are expected to increase as T_e/kT_s increases. This has been indeed observed in our simulations, see Fig.2a.

The PIC results for the escaping thermionic current and the virtual cathode depth as a function of the surface temperature have been plotted in Fig.2 together with the predictions of the Takamura model. In all the simulated scenarios, the escaping thermionic current is equal to the nominal Richardson current up to a plasma-dependent plateau and then becomes nearly independent of the surface temperature; it exhibits small fluctuations around a mean value that corresponds to the space-charge limited current. The exact limited current should increase as the surface temperature increases because the emitted electrons become progressively faster - this increase is very small and monotonic, which implies that the observed fluctuations

are mainly of numerical origin. There is a remarkable agreement of $j_{\rm th}^{\rm esc}$ and $\Phi_{\rm vc}$ with the Takamura analytical model. The PIC results for $j_{\rm th}^{\rm esc}$ are consistently only slightly higher than the theoretical predictions, most probably due to the cold ion assumption of Takamura.

The space-charge limited current $j_{\rm th}^{\rm lim}$ should strongly depend on the plasma density and temperature, but slightly depend on the surface temperature. Neglecting the latter dependence for $T_{\rm s} = 0$, $j_{\rm th}^{\rm lim}$ stemming from the Takamura model has been fitted to a modified Child-Langmuir formula in Ref.[18]. In the spirit of such normalizations, our comprehensive PIC results for AUG reveal that the ratio of the limited current $j_{\rm th}^{\rm lim}$ over the "thermal" plasma electron current $en_{\rm e}v_{\rm Te}$ is approximately constant and equal to 0.430, whereas the modified Child-Langmuir formula predicts 0.364 (15% discrepancy). A more detailed comparison with different variants of the Takamura model is featured in Table 1. We conclude that the finite-$T_{\rm s}$ model is very accurate in spite of the cold ion assumption, whereas its $T_{\rm s} = 0$ limit as well as the modified Child-Langmuir formula are rather crude especially for the inter-ELM case that is characterized by the smallest $T_{\rm e}/kT_{\rm s}$ ratio. Finally, we emphasize that the simple relation $j_{\rm th}^{\rm lim} = 0.430en_{\rm e}v_{\rm Te}$ can be employed for the modelling of thermionic suppression above any surface point of the leading edge that is subject to the spatio-temporal ELM profile.

Let us now briefly justify why we neglected the Schottky effect, *i.e.* the enhancement of the thermionic current in the presence of accelerating - for the emitted electrons - electrostatic fields. Mathematically, the Schottky effect is equivalent to the effective lowering of the work-function by $\Delta W_{\rm f} = \sqrt{e^3 E_{\rm w}}$ in cgs units, where $E_{\rm w} > 0$ is the accelerating electric field at the wall [19]. It is evident that there is no Schottky effect for the space-charge limited regime due to $E_{\rm w} \leq 0$. Prior to current limitation, $E_{\rm w}$ and thus $\Delta W_{\rm f}$ will be maximum for normal magnetic fields and intra-ELM plasma conditions. Upper bound estimates can be found by neglecting the presence of thermionic electrons and employing $E_{\rm w} \simeq |\phi_{\rm pl} - \phi_{\rm s}|/\lambda_{\rm De}$. They yield $E_{\rm w} \simeq 2.4 \times 10^7$ V/m, which translates to $\Delta W_{\rm f} \simeq 0.186$ eV. The PIC simulations, for $T_{\rm s} = 3400$ K, yield $E_{\rm w} \simeq 1.12 \times 10^7$ V/m, which translates to $\Delta W_{\rm f} \simeq 0.125$ eV. Hence, the Schottky effect is inactive in the space-charge limited regime, whereas in the Richardson-Dushman regime - even in the worst case scenario - it leads to a work-function decrease that is comparable to uncertainties due to surface impurities and local crystallographic variations [20].

Table 1. The space-charge limited current $j_{\rm th}^{\rm lim}$ for the leading edge geometry in absolute units and normalized by $en_{\rm e}v_{\rm Te}$ according to the PIC simulations (averaged due to the numerical fluctuations), the finite-$T_{\rm s}$ Takamura model (averaged over the simulated surface temperatures due to the slight $T_{\rm s}$ dependence) and the $T_{\rm s} = 0$ limit of the Takamura model [17].

$j_{\rm th}^{\rm lim}$	PIC (MA/m^2)	$T_{\rm s} \neq 0$ (MA/m^2)	$T_{\rm s} = 0$ (MA/m^2)	PIC ($en_{\rm e}v_{\rm Te}$)	$T_{\rm s} \neq 0$ ($en_{\rm e}v_{\rm Te}$)	$T_{\rm s} = 0$ ($en_{\rm e}v_{\rm Te}$)
inter-ELM	4.416	4.262	3.903	0.439	0.424	0.388
reduced intra-ELM	8.860	8.523	8.061	0.427	0.410	0.388
intra-ELM	11.42	10.88	10.41	0.426	0.406	0.388

4. Sloped geometry

For oblique magnetic field incidence, there are no analytical models capable of describing thermionic suppression due to the interplay of space-charge effects and prompt re-deposition. The PIC results for the escaping thermionic current and the virtual cathode depth as a function of the surface temperature have been plotted in Fig.3. Similar to the leading edge geometry, the escaping current closely follows the nominal Richardson current up to a certain surface temperature and then becomes nearly constant, whereas - after its emergence - the normalized virtual cathode depth $\Phi_{\rm vc}/kT_{\rm s}$ is almost linearly increasing with $T_{\rm s}$.

In lack of an analytical theory, the following qualitative remarks are appropriate: **(i)** The agreement with the Richardson-Dushman formula prior to the formation of the virtual cathode suggests that prompt re-deposition is negligible when the potential profile is monotonic. This implies that the sheath electric field in the proximity of the surface effectively accelerates the emerging thermionic electrons away from the material boundary and thus prevents reabsorption during their first gyro-period. This can be explained by considering the large $T_{\rm e}/kT_{\rm s}$ ratios of our simulations that correspond to large electrostatic over Lorentz force ratios [21, 22]. **(ii)** As $T_{\rm s}$ increases, the electrostatic field near the surface gradually decreases and inverts its sign after the virtual cathode is formed. In this manner, the competition between the electrostatic and the Lorentz force turns to synergy and space-charge effects enhance prompt re-deposition. The effectiveness of these two entangled mechanisms is reflected on the smaller limited current $j_{\rm th}^{\rm lim}/\sin\alpha$ (including magnetic field compression) compared to the leading edge geometry under the same plasma scenarios. **(iii)** It is worth noting that the expression $j_{\rm th}^{\rm nom}\exp\left(-e\Phi_{\rm vc}/kT_{\rm s}\right)$ no longer provides the total escaping thermionic current but the relation $j_{\rm th}^{\rm nom}\exp\left(-e\Phi_{\rm vc}/kT_{\rm s}\right) - j_{\rm th}^{\rm esc}$ can be employed for a rough estimate of the contribution of prompt re-deposition to thermionic suppression. For the plasma conditions considered, most thermionic electrons are re-absorbed being unable to overcome the potential barrier and not owing to their gyration. **(iv)** In spite of prompt re-deposition, the escaping

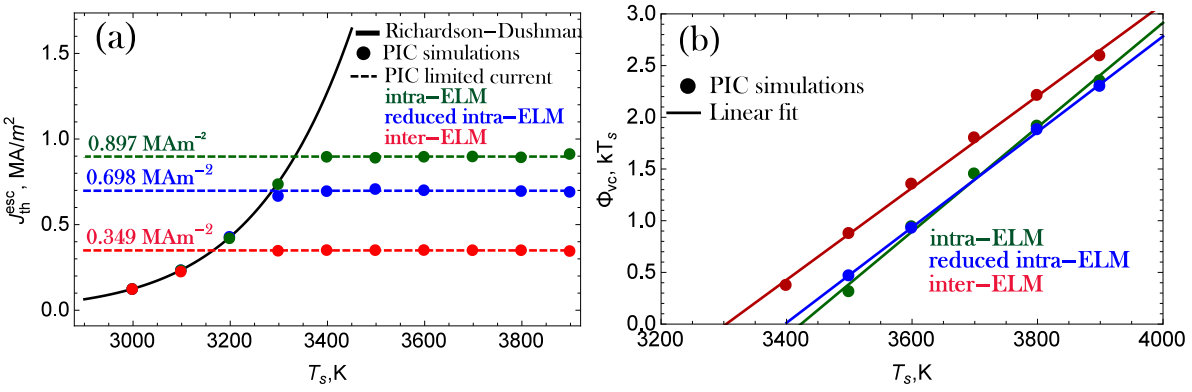

Figure 3. Sloped geometry results of the PIC simulations for the selected plasma scenarios. (a) The escaping thermionic current as computed by the particle counting method (•) and the average limited current (dashed lines). (b) The virtual cathode depth normalized by the surface temperature (•) and its linear least-squares fit (continuous lines).

thermionic current becomes strictly limited as the material temperature increases, albeit for lower surface temperatures and thus at much lower values compared to the leading edge, approximately 15 times smaller.

The limited current $j_{\mathrm{th}}^{\mathrm{lim}}$ should strongly depend on the plasma density and temperature (but also on the magnetic field strength and inclination angle, which are constant here). Following the reasoning of the previous section, it is worth to investigate whether the ratio of the limited current $j_{\mathrm{th}}^{\mathrm{lim}}$ over the "thermal" plasma electron current $en_{\mathrm{e}}v_{\mathrm{Te}}\sin\alpha$ (including spreading by the magnetic field) is nearly constant. For inter-ELM plasmas the ratio becomes 0.115, for intra-ELM plasmas the ratio becomes 0.111 and for reduced intra-ELM plasmas the ratio becomes 0.112. We thus suggest that a simple approximate relation $j_{\mathrm{th}}^{\mathrm{lim}} = 0.113en_{\mathrm{e}}v_{\mathrm{Te}}\sin\alpha$ is employed for the modelling of thermionic suppression above any surface point of the sloped lamella that is subject to the spatio-temporal ELM profile. However, more PIC simulations for different plasma scenarios need to be performed to confirm the generality of the proposed scaling.

5. Conclusions

The electrostatic sheath and magnetic pre-sheath of thermionically emitting perfectly planar tungsten surfaces has been simulated with the 2D3V SPICE2 PIC code for plasma conditions relevant to inter- and intra-ELM periods of the AUG divertor. Normal ($\alpha = 90°$) and oblique ($\alpha = 17.5°$) magnetic field orientations were considered that correspond to the leading edge and the sloped lamella geometries. *For the leading edge*, the PIC results for the space-charge limited current and the virtual cathode depth agree exceptionally well with the predictions of the Takamura model for finite surface temperatures and cold ions [17]. Deviations from the theory due to the finite ion temperature are hardly distinguishable. *For the sloped geometry*, the PIC results have revealed that the escaping thermionic current matches the Richardson-Dushman formula up to a limiting value, which is much smaller than in the leading edge. This implies that prompt re-deposition contributes to thermionic suppression only once the virtual cathode has formed, since the Lorentz force cannot compete with the repulsive electrostatic sheath force as a consequence of the very low initial speed of the emitted electrons.

The ratio of the limited current stemming from PIC simulations over the thermal electron current was observed to be nearly constant (for given inclination angle, magnetic field strength and sheath potential drop) under both inter- and intra-ELM conditions. Based on this proportionality, analytical formulas were proposed that allow for an accurate description of thermionic suppression for arbitrary plasma densities and temperatures in both exposure geometries. These results suggest that stable sheath formation leads to the establishment of a limited escaping current also for oblique magnetic field inclination angles. More extensive PIC simulations, especially for grazing magnetic field incidence, are required in order to verify this conjecture. This will be the subject of future work.

Acknowledgments

This work was supported by the Czech Science Foundation project GA16-14228S and co-funded by MEYS, projects number 8D15001 and LM2015070. The simulations reported have been performed at the National Computational Center IT4Innovations and MARCONI. We acknowledge the CINECA award under the ISCRA initiative, for the availability of high performance computing resources and support. This work has also been carried out within the framework of the EUROfusion Consortium and has received funding from the Euratom research and training programme 2014-2018 under grant agreement No 633053. The work was performed under WP PFC. The views and opinions expressed herein do not necessarily reflect those of the European Commission or of the ITER Organization. ITER is the nuclear facility INB 174. P. T. and S. R. would also like to acknowledge the financial support of the Swedish Research Council.

[1] Pitts R A, Bardin S, Bazylev B, van den Berg M A et al. 2017 Physics conclusions in support of ITER W divertor monoblock shaping *Nucl. Mat. Energy* http://dx.doi.org/10.1016/j.nme.2017.03.005
[2] Coenen J W, Arnoux G, Bazylev B, Matthews G F *et al.* 2015 *Nucl. Fusion* **55** 023010
[3] Coenen J W, Arnoux G, Bazylev B, Matthews G F *et al.* 2015 *J. Nucl. Mater.* **463** 78
[4] Krieger K, Coenen J W, Matthews G F, Sieglin B *et al.* 2017 *Nucl. Fusion* (submitted)
[5] Krieger K, Sieglin B, Balden M, Coenen J W *et al.* 2017 *Phys. Scr.* (these proceedings)
[6] Herring C and Nichols M H 1949 *Rev. Mod. Phys.* **21** 185
[7] Michaelson H B 1977 *J. Appl. Phys.* **48** 4729
[8] Fomenko V 1966 *Handbook of Thermionic Properties: Electronic Work Functions & Richardson Constants of Elements and Compounds* (New York: Plenum)
[9] Benilov M S 2009 *Plasma Sources Sci. Technol.* **18** 014005
[10] Robertson S 2013 *Plasma Phys. Control. Fusion* **55** 093001
[11] Dejarnac R and Gunn J P 2007 *J. Nucl. Mater.* **363-365** 560
[12] Komm M, Dejarnac R, Gunn J P, Kirschner A *et al.* 2011 *Plasma Phys. Control. Fusion* **53** 115004
[13] Komm M, Ratynskaia S, Tolias P, Cavalier J *et al.* 2017 *Plasma Phys. Control. Fusion* **59** 094002
[14] Bazylev B, Janeschitz G, Landman I, Loarte A *et al.* 2009 *J. Nucl. Mater.* **390-391** 810
[15] Thorén E, Bazylev B, Ratynskaia S, Tolias P *et al.* 2017 *Phys. Scr.* **T170** 014006
[16] Tskhakaya D, Jachmich S, Eich T, Fundamenski W *et al.* 2011 *J. Nucl. Mater.* **415** S860
[17] Takamura S, Ohno N, Ye M Y and Kuwabara T 2004 *Contrib. Plasma Phys.* **44** 126
[18] Hagino Y, Ohno N and Takamura S 2004 *Contrib. Plasma Phys.* **44** 144
[19] Nottingham W B 1956 Thermionic emission *Handbuch der Physik Volume XXI: Electron Emission and Gas Discharges* ed S Flügge (Berlin: Springer-Verlag)
[20] Czack G, Kirschstein G, Kurtz W and Stein F 1993 *Gmelin Handbook of Inorganic and Organometallic Chemistry, Tungsten, Supplement Volume A4* (Berlin: Springer-Verlag)
[21] Tskhakaya D and Kuhn S 2000 *Contrib. Plasma Phys.* **40** 484
[22] Takamura S, Mizoshita S and Ohno N 1996 *Phys. Plasmas* **3** 4310